CELL BIOLOGY

Heat shock protein 27 activity is linked to endothelial barrier recovery after proinflammatory GPCR-induced disruption

Cara C. Rada[1,2], Hilda Mejia-Pena[1], Neil J. Grimsey[3], Isabel Canto Cordova[1,2], Joshua Olson[4], Jacob M. Wozniak[1,2,5], David J. Gonzalez[1,5], Victor Nizet[4,5], JoAnn Trejo[1]*

Vascular inflammation causes endothelial barrier disruption and tissue edema. Several inflammatory mediators act through G protein–coupled receptors (GPCRs), including protease-activated receptor-1 (PAR1), to elicit inflammatory responses. The activation of PAR1 by its ligand thrombin stimulates proinflammatory, p38 mitogen-activated protein kinase (MAPK) signaling that promotes endothelial barrier disruption. Through mass spectrometry phosphoproteomics, we identified heat shock protein 27 (HSP27), which exists as a large oligomer that binds to actin, as a promising candidate for the p38-mediated regulation of barrier integrity. Depletion of HSP27 by siRNA enhanced endothelial cell barrier permeability and slowed recovery after thrombin stimulation. We further showed that two effector kinases of p38 MAPK, MAPKAPK2 (MK2) and MAPKAPK3 (MK3), differentially phosphorylated HSP27 at Ser[15], Ser[78], and Ser[82]. Whereas inhibition of thrombin-stimulated p38 activation blocked HSP27 phosphorylation at all three sites, inhibition of MK2 reduced the phosphorylation of only Ser[15] and Ser[78]. Inhibition of both MK2 and MK3 was necessary to attenuate Ser[82] phosphorylation. Thrombin-stimulated p38-MK2-MK3 signaling induced HSP27 oligomer disassembly. However, a phosphorylation-deficient mutant of HSP27 exhibited defective oligomer disassembly and altered the dynamics of barrier recovery after thrombin stimulation. Moreover, blocking HSP27 oligomer reassembly with the small-molecule inhibitor J2 enhanced endothelial barrier permeability in vitro and vascular leakage in vivo in response to PAR1 activation. These studies reveal the distinct regulation of HSP27 phosphorylation and function induced by the GPCR-stimulated p38-MK2-MK3 signaling axis that controls the dynamics of endothelial barrier recovery in vitro and vascular leakage in vivo.

INTRODUCTION

Vascular endothelial cells form a semipermeable barrier that is important for normal tissue homeostasis. Disruption of the endothelial barrier by inflammatory mediators leads to increased permeability, tissue edema, and subsequent organ failure (1). Many inflammatory mediators act through G protein–coupled receptors (GPCRs) to promote endothelial barrier disruption (2); however, the mechanism by which this occurs is not clearly understood. Protease-activated receptor-1 (PAR1), a GPCR for the protease thrombin, couples to $G\alpha_q$ and $G\alpha_{12/13}$ proteins and causes transient endothelial barrier disruption through increases in intracellular Ca^{2+} and activation of protein kinase C and RhoA (1). These pathways converge on myosin light-chain (MLC) phosphorylation, which promotes actin-myosin contractility and adherens junction disassembly, resulting in endothelial barrier permeability.

We and others have shown a role for p38 mitogen-activated protein kinase (MAPK), in addition to the classic GPCR effectors, in endothelial barrier disruption induced by thrombin (3, 4). We demonstrated that thrombin-dependent activation of PAR1 stimulates p38 MAPK signaling independently of the canonical, three-tiered kinase cascade and, instead, occurs through a noncanonical pathway mediated by transforming growth factor–β–activated kinase-1

binding protein-1 (TAB1) (4, 5). In addition, multiple other GPCRs, including the H1 histamine receptor, activate p38 through the noncanonical, TAB1-dependent pathway in endothelial cells (5). We further showed that noncanonical activation of p38 signaling induced by thrombin-activated PAR1 promotes endothelial permeability (4). Similarly, other GPCRs, including the H1 receptor, also signal through p38 to promote endothelial barrier disruption (6); however, there is limited knowledge regarding the mechanisms by which GPCR-activated p38 MAPK signaling regulates endothelial barrier disruption.

Heat shock protein 27 (HSP27) is a small molecular chaperone that forms large oligomers that bind to monomeric actin and prevent actin polymerization (7, 8). Phosphorylation of HSP27 causes the disassembly of large oligomers and the release of actin, which promotes actin polymerization (8, 9). These findings suggest that HSP27 contributes to endothelial barrier disruption through modulation of actin-myosin contractility. However, overexpression of HSP27 suppresses actin polymerization and preserves blood-brain barrier integrity, suggesting a counter-regulatory role for HSP27 that promotes endothelial barrier stabilization (10). HSP27 is a downstream target of p38 signaling (11); however, the role of HSP27 in GPCR-induced endothelial barrier disruption has not been previously examined.

In this study, we report that thrombin-activated, PAR1-induced p38 MAPK signaling was not integrated with the RhoA-MLC pathway and, instead, acted through an MK2-MK3-HSP27 signaling axis to enhance endothelial barrier integrity. Activation of the p38-mediated MK2-MK3-HSP27 signaling axis is also conserved for other endothelial GPCRs. We further showed that HSP27 acted in a counter-regulatory role and recovery endothelial barrier permeability induced by thrombin. GPCR regulation of HSP27 activity required MK2- and MK3-mediated HSP27 phosphorylation at distinct sites,

[1]Department of Pharmacology, University of California, San Diego, La Jolla, CA 92093, USA. [2]Biomedical Sciences Graduate Program, University of California, San Diego, La Jolla, CA 92093, USA. [3]Department of Pharmaceutical and Biomedical Sciences, University of Georgia, Athens, GA 30682, USA. [4]Department of Pediatrics, University of California, San Diego, La Jolla, CA 92093, USA. [5]Skaggs School of Pharmacy and Pharmaceutical Sciences, University of California, San Diego, La Jolla, CA 92093, USA.
*Corresponding author. Email: joanntrejo@ucsd.edu

which controlled the dynamics of HSP27 oligomerization and endothelial barrier recovery. Furthermore, inhibition of HSP27 oligomer reassembly with J2 enhanced thrombin-stimulated endothelial barrier permeability in vitro, and J2 also increased PAR1-induced vascular leakage in vivo.

RESULTS
Thrombin-induced p38 signaling is not integrated with the RhoA-MLC pathway but promotes HSP27 phosphorylation

The mechanism by which p38 signaling contributes to endothelial barrier disruption induced by GPCRs is not known. To assess whether thrombin-activated p38 signaling was integrated with the RhoA-MLC signaling pathway, we tested the effect of p38 blockade on the activation of RhoA and the phosphorylation of MLC, which are downstream effectors of $G\alpha_q$ and $G\alpha_{12/13}$ signaling. Thrombin induced a rapid and substantial increase in RhoA activation in human umbilical vein endothelial cell (HUVEC)–derived EA.hy926 cells in vehicle-treated control cells (Fig. 1A, top, lanes 1 and 2), whereas inhibition of p38 with SB203580, a selective inhibitor of p38α and p38β, had no effect on RhoA activation (Fig. 1A, top, lanes 3 and 4). Phosphorylation of MLC, an MLC kinase substrate regulated by RhoA and Ca^{2+}, peaked after 1 min of thrombin stimulation in HUVECs and then declined (Fig. 1B, lanes 1 to 6). A similar change in MLC phosphorylation was observed in cells treated with SB203580 (Fig. 1B, lanes 7 to 12), suggesting that thrombin-induced RhoA signaling was not dependent on p38 activation. Next, we determined whether p38 signaling was dependent on RhoA activation in response to thrombin. Endothelial EA.hy926 cells were pretreated with the p38 inhibitor SB203580 or Fasudil, a specific inhibitor of the RhoA effector Rho-associated protein kinase (ROCK), alone or in combination and then were stimulated with thrombin. Thrombin-induced p38 phosphorylation was significantly inhibited by SB203580, but this failed to affect phosphorylation of the ROCK substrate myosin phosphatase target subunit 1 (MYPT1) compared with that in the dimethyl sulfoxide (DMSO)–treated control (fig. S1, lanes 1 to 6). Conversely, inhibition of ROCK with Fasudil had no effect on thrombin-stimulated p38 phosphorylation but significantly decreased MYPT1 phosphorylation compared to that in the DMSO-treated control cells (fig. S1, lanes 1 to 3 versus lanes 7 to 10). These data suggest that the thrombin-stimulated activation of p38 and RhoA signaling are not interdependent. As expected, SB203589 and Fasudil blocked both p38 and MYPT1 phosphorylation (fig. S1, lanes 10 to 12).

To identify previously uncharacterized downstream mediators of thrombin-activated p38 signaling, a quantitative phosphoproteomics analysis of thrombin-stimulated endothelial EA.hy926 cells (12) was examined and HSP27 emerged as a promising candidate. HSP27 was previously implicated in the regulation of endothelial barrier integrity (10, 13, 14). Incubation of EA.hy926 cells with thrombin for 2.5 or 5 min resulted in a significant increase in HSP27 phosphopeptide abundance containing four distinct sites, including Ser[15], Ser[78], Ser[82], and Ser[83] (Fig. 1, C and D). The HSP27 Ser[15] and Ser[82] phosphosites present in thrombin-stimulated cells were detected on single peptides, whereas the Ser[78] phospho-site was only detected together with the Ser[82] phospho-site or both the Ser[82] and Ser[83] phospho-sites (Fig. 1, C and D). HSP27 phosphorylation at Ser[15], Ser[78], and Ser[82] affects HSP27 function (11), but whether GPCR-stimulated HSP27 phosphorylation regulates endothelial barrier integrity is not known and was examined.

GPCR agonists stimulate p38-dependent HSP27 phosphorylation in multiple endothelial cell types

To better understand HSP27 function, we examined the kinetics of thrombin-induced HSP27 phosphorylation. HUVECs were stimulated with thrombin over a 60-min time course, and phosphorylation of HSP27 on Ser[15], Ser[78], and Ser[82] was detected with phospho-specific HSP27 antibodies. Thrombin increased HSP27 phosphorylation at all three sites with varying kinetics. Ser[15] phosphorylation peaked between 10 and 30 min after thrombin stimulation (Fig. 2A, lanes 1 to 6). A peak in Ser[78] phosphorylation was detected at 10 min after thrombin incubation (Fig. 2A, lanes 1 to 6), whereas Ser[82] phosphorylation was detected at 5 min and remained increased in thrombin-treated cells (Fig. 2A, lanes 1 to 6). To examine whether thrombin-stimulated HSP27 phosphorylation required PAR1, HUVECs were pretreated with the PAR1-selective antagonist vorapaxar. In vorapaxar-treated cells, thrombin-induced HSP27 phosphorylation at all three sites was significantly inhibited compared to that in DMSO-treated control cells (fig. S2A, lanes 1 to 3 versus lanes 4 to 6). Similarly to thrombin, the PAR1-specific agonist peptide TFLLRNPNDK significantly increased HSP27 phosphorylation at all three sites in control HUVECs (fig. S2B, lanes 1 to 3), which was blocked by vorapaxar (fig. S2B, lanes 4 to 6). Thus, the thrombin-dependent activation of PAR1 promoted HSP27 phosphorylation in cultured human endothelial cells.

To determine whether the thrombin-induced phosphorylation of HSP27 required p38 activity, HUVECs were pretreated with SB203580. Inhibition of p38 caused a significant reduction in thrombin-stimulated HSP27 phosphorylation at Ser[15] and Ser[78], whereas a modest but significant decrease in Ser[82] phosphorylation was observed compared to that in DMSO-treated control cells (Fig. 2A, lanes 1 to 6 versus lanes 7 to 12). Next, the role of the p38α isoform in thrombin-stimulated HSP27 phosphorylation was assessed by small interfering RNA (siRNA)–targeted depletion. Depletion of p38α blocked thrombin-induced phosphorylation of HSP27 Ser[78] and Ser[15] compared to that in HUVECs transfected with nonspecific siRNA (fig. S3, lanes 1 to 6 versus lanes 7 to 12). However, in contrast to the effects of SB203580, depletion of p38α failed to significantly inhibit the thrombin-induced phosphorylation of HSP27 at Ser[82] (fig. S3), suggesting that residual p38α, the p38β isoform, or another kinase was sufficient to phosphorylate HSP27 at Ser[82] under these conditions.

Thrombin-dependent HSP27 phosphorylation was next examined in primary human dermal microvascular endothelial cells (HDMECs) to determine whether the pathway was conserved in other endothelial cell types. HDMECs were stimulated with thrombin over a 60-min time course, and HSP27 phosphorylation was determined. Thrombin caused a peak in phosphorylation of HSP27 Ser[78] and Ser[82] at 5 and 10 min, respectively, which remained increased and then declined (Fig. 2B, lanes 1 to 6). HSP27 Ser[15] phosphorylation peaked at 5 min and was sustained for 60 min after thrombin incubation (Fig. 2B, lanes 1 to 6). Pretreatment with the p38 inhibitor SB203580 significantly inhibited thrombin-induced HSP27 Ser[15] and Ser[78] phosphorylation and modestly but significantly reduced Ser[82] phosphorylation (Fig. 2B, lanes 7 to 12). In HUVECs and HDMECs, thrombin-induced HSP27 phosphorylation was substantially inhibited by SB203580, suggesting that p38-mediated regulation of HSP27 phosphorylation functions in more than one endothelial cell type.
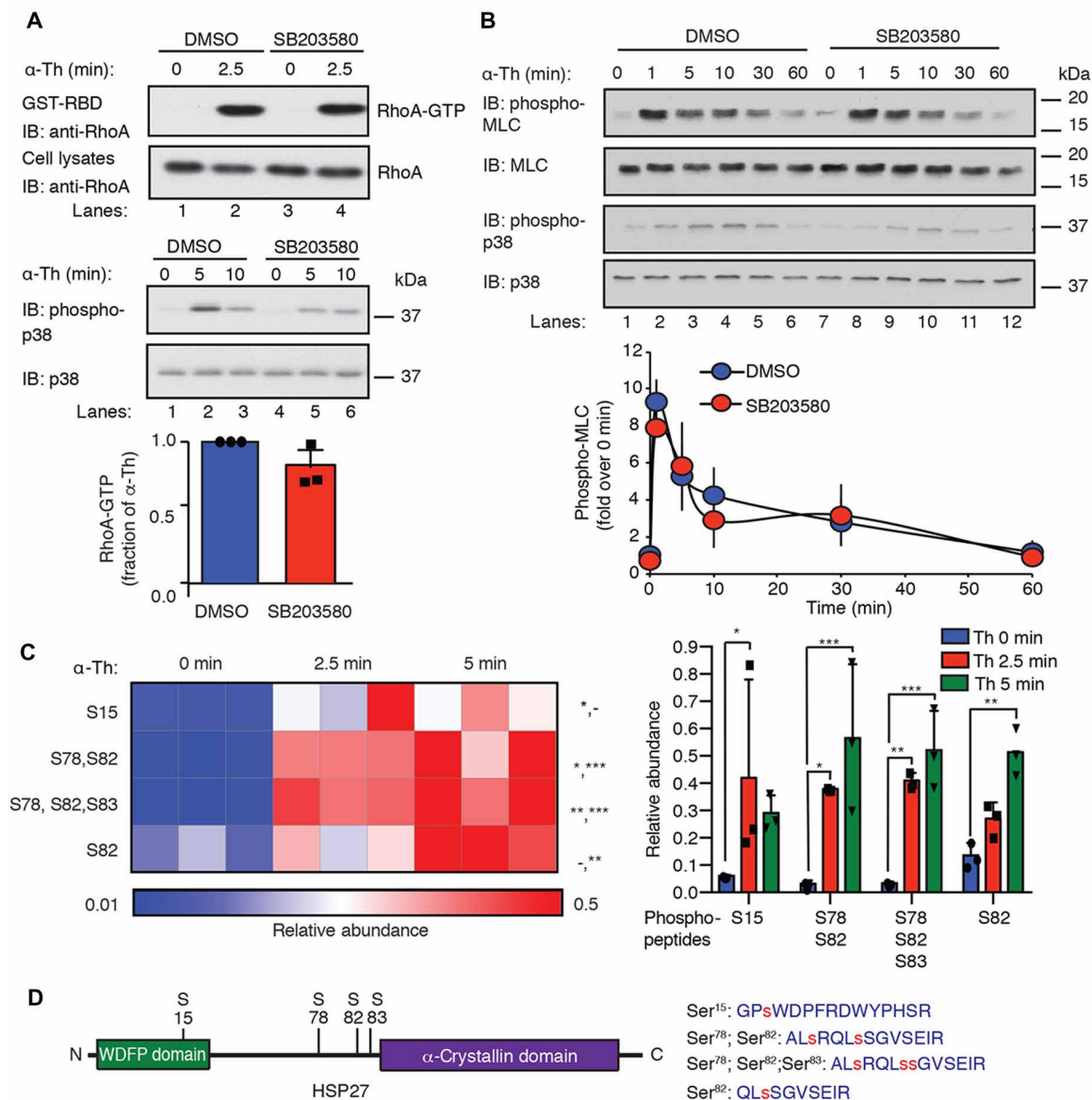
Fig. 1. Thrombin-induced p38 signaling is independent of the RhoA-MLC pathway and promotes HSP27 phosphorylation. (A) Top: Assessment of RhoA activity in EA.hy926 cells pretreated with the 3 μM SB203580 (p38 inhibitor) or DMSO for 1 hour and stimulated with 10 nM thrombin (α-Th). Blots of RhoA and p38 are representative of three independent experiments. Bottom: Data in the bar graph are means ± SD of three independent experiments and were analyzed by Student's t test (not significant). **(B)** Top: Immunoblotting (IB) analysis of total and phosphorylated MLC and p38 in HUVECs pretreated with SB203580 or DMSO and then stimulated with α-Th for the indicated times. Blots are representative of three independent experiments. Bottom: Densitometric analysis of the fold change in the relative abundances of the indicated phosphorylated proteins over time. Data are means ± SD of three independent experiments and were analyzed by Student's t test (not significant). **(C)** Left: Heatmap of HSP27 phospho-peptide site abundance induced by α-Th over time. Data were derived from three biological replicates. Increases and decreases in phospho-peptide abundance are indicated by the red and blue color intensities, respectively. Color intensities depict phospho-peptide abundances in each row induced by α-Th relative to the respective zero-time control. Right: Changes in HSP27 phospho-peptide abundance at the indicated times. Data were analyzed by two-way analysis of variance (ANOVA). *$P < 0.05$; **$P < 0.01$; ***$P < 0.001$; -, not significant. **(D)** Left: Schematic of HSP27 containing an N-terminal WDFP motif and a C-terminal α-crystallin domain. Right: HSP27 phospho-peptides identified by MS analysis, where phosphorylated serine residues are indicated by the red "s."

Histamine signals through its H1 and H2 GPCRs expressed in endothelial cells and promotes barrier disruption (6). To determine whether other GPCR agonists stimulated HSP27 phosphorylation, HUVECs were stimulated with histamine over a 30-min time course. Histamine induced a peak in the phosphorylation of HSP27 at Ser[15], Ser[78], and Ser[82] at 10 min (Fig. 2C, lanes 1 to 5), which then declined

to baseline by 30 min. Pretreatment with SB203580 completely ablated the histamine-stimulated phosphorylation of HSP27 at Ser[15], Ser[78], and Ser[82] (Fig. 2C, lanes 6 to 10). Similarly to thrombin, histamine promoted p38-dependent HSP27 phosphorylation at all three phosphosites. These findings indicate that multiple endothelial GPCRs induce HSP27 phosphorylation through a p38-dependent pathway.
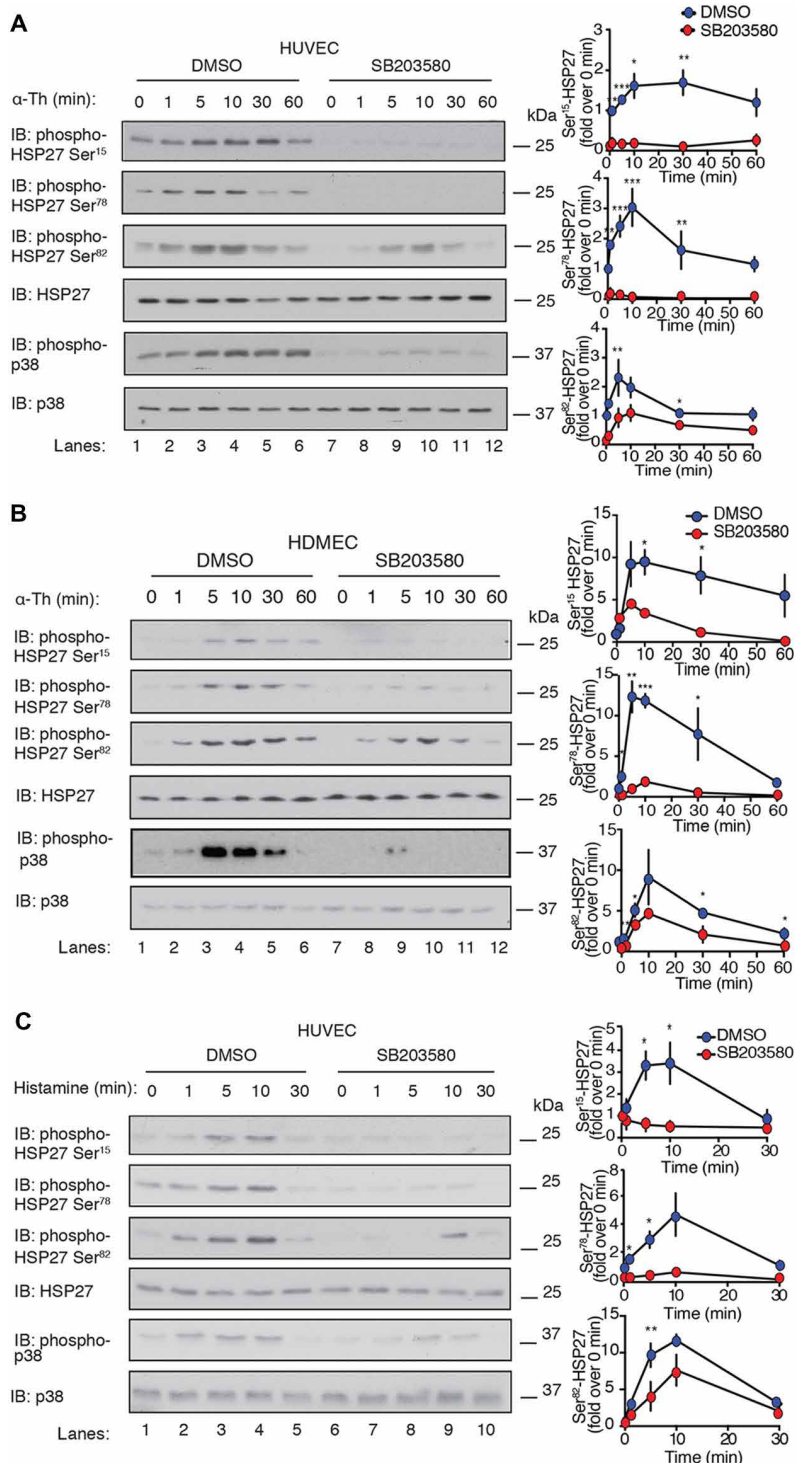
Fig. 2. GPCR agonists stimulate p38-dependent HSP27 phosphorylation in different endothelial cell types. (**A** and **B**) Left: Immunoblotting analysis of phosphorylated HSP27 and p38 induced by 10 nM thrombin (α-Th) at the indicated times in (A) HUVECs or (B) HDMECs pretreated for 1 hour with 3 μM SB203580 or DMSO. (**C**) Left: Immunoblotting analysis of phosphorylated HSP27 and p38 induced by 10 μM histamine at the indicated times in HUVECs pretreated with SB203580 or DMSO. Blots in (A) to (C) are representative of four independent experiments. (A to C) Right: Densitometric analysis of the fold change in the relative abundances of the indicated phosphorylated proteins over time. Data are means ± SD of four independent experiments and were analyzed by Student's t test. *P < 0.05; **P < 0.01; ***P < 0.001.

HSP27 depletion enhances thrombin-induced endothelial barrier permeability in vitro

In previous studies, we showed that p38 signaling mediates thrombin-stimulated endothelial permeability in vitro and PAR1-induced vascular leakage in vivo (4). HSP27 also modulates endothelial barrier in vitro (13) and in vivo (10); however, the role of HSP27 in thrombin-induced endothelial barrier permeability is not known. To examine the function of HSP27 in thrombin-stimulated barrier disruption, HUVECs were transfected with HSP27-specific or nonspecific siRNAs and then stimulated with thrombin for 10 min, and the flux of Evans blue–bound albumin across the cell monolayer was quantified over time. In HUVECs transfected with nonspecific siRNA, thrombin increased endothelial barrier permeability based on the accumulation of Evans blue–bound albumin that peaked at 10 min compared to that in untreated control cells (Fig. 3, A and B), consistent with our previous reports (4, 15, 16). Unexpectedly, however, in HUVECs depleted of HSP27, thrombin caused a 2.5-fold greater increase in endothelial barrier permeability at 30 min compared to that in control cells transfected with nonspecific siRNA (Fig. 3, A and B). These findings indicate that HSP27 has a role in regulating thrombin-induced endothelial barrier permeability.

GPCR-stimulated endothelial barrier disruption is rapid, transient, and reversible. To determine more precisely how the loss of HSP27 affected endothelial barrier dynamics, we used real-time, electric cell-substrate impedance sensing (ECIS). ECIS monitors the dynamics of barrier function, including the maximum change in impedance or barrier function, the time to maximum change in impedance, and the time to barrier recovery. HDMECs form strong cell-cell junctions that recapitulate the primary barrier and were used to examine HSP27 function in endothelial barrier dynamics. In HDMECs transfected with nonspecific siRNA, thrombin caused a rapid, 20% reduction in impedance (barrier function) that peaked at ~4 min (Fig. 3, C to E), which was followed by a rapid recovery that returned to baseline by ~40 min (Fig. 3, C and F). In contrast, HDMECs deficient in HSP27 exhibited a greater, 30% reduction in impedance from baseline after exposure to thrombin, with the maximum loss of barrier function at ~10 min (Fig. 3, C to E). Moreover, in HSP27-depleted HDMECs, the time to recovery was more prolonged, occurring ~60 min after thrombin stimulation, compared to that in cells transfected with nonspecific siRNA (Fig. 3, C and F). Depletion of HSP27 had no significant effect on baseline basal barrier function (Fig. 3, A and C). Because the loss of HSP27 function did not alter baseline barrier function or the capacity of thrombin to initiate barrier disruption, HSP27 appears to function primarily in controlling barrier recovery after thrombin stimulation.

MK2 and MK3 are required for the thrombin-induced phosphorylation of HSP27

GPCR-stimulated HSP27 phosphorylation is dependent on p38 MAPK; however, HSP27 is not a direct substrate of p38
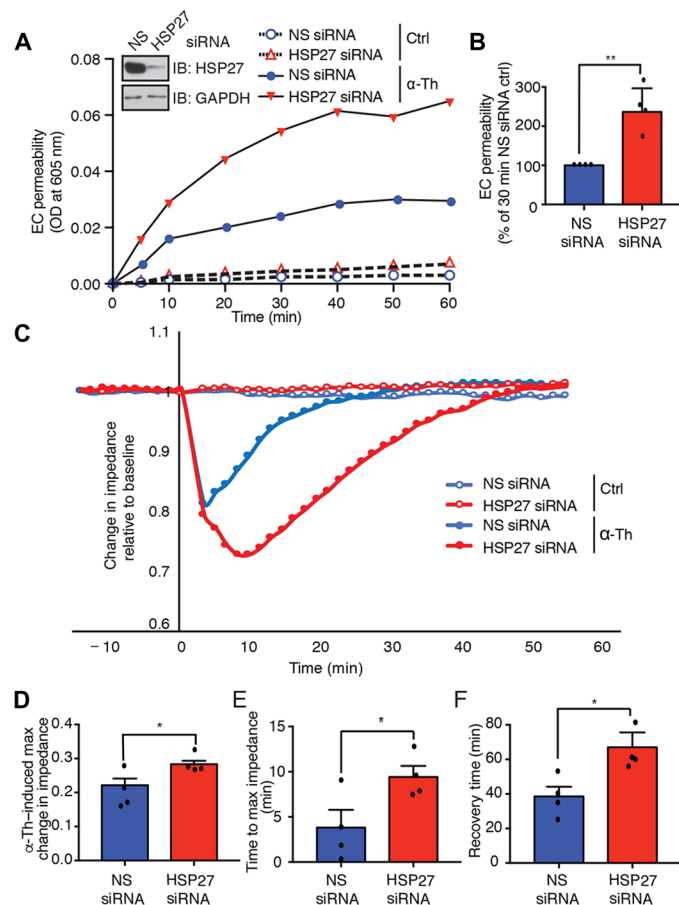
Fig. 3. Depletion of HSP27 enhances thrombin-induced endothelial barrier permeability in vitro. (**A**) Endothelial cell (EC) barrier permeability was examined in HUVECs that were transfected with HSP27-specific or nonspecific (NS) siRNAs and stimulated with or without 10 nM thrombin (α-Th) for 10 min. The flux of Evans blue albumin diffusion was measured over time. Inset: Immunoblotting analysis of siRNA-targeted HSP27 depletion. OD, optical density. (**B**) Quantification of α-Th–induced EC permeability determined at 30 min from four independent experiments each performed in duplicate. Data are means ± SEM and were analyzed by Student's *t* test. **P < 0.01. (**C**) Endothelial barrier impedance or function in HDMECs transfected with HSP27-specific or NS siRNA and then stimulated with α-Th was measured by ECIS. (**D** to **F**) The barrier impedance data were normalized to baseline for each condition, and the maximum (max) α-Th–induced change in impedance (D), time to max impedance (E), and time to barrier recovery (F) were quantified from four independent experiments each performed in duplicate. Data are means ± SEM and were analyzed by two-way ANOVA and Dunnett's posttests. *P < 0.05.

but rather a substrate of effector kinases downstream of p38 (*11*). To determine which p38-regulated kinases mediated thrombin-stimulated HSP27 phosphorylation, we used PHOXTRACK (PHOsphosite-X-TRacing Analysis of Causal Kinases) computational software (*17*) to interrogate the thrombin-induced phosphoproteome (*12*) and identified two candidates, MAPKAPK2 (MK2) and MAPKAPK3 (MK3), as potential HSP27 causal kinases (fig. S4A). A previous study showed that MK2 activity is modulated by thrombin in endothelial cells (*18*), supporting a role for MK2. Moreover, MK2 directly phosphorylates HSP27 in platelets (*19*), vascular smooth muscle cells (*20*), and in vitro in experiments with purified proteins (*21*). MK3

also directly phosphorylates HSP27 in vitro (*11*, *22*). However, neither MK2 nor MK3 has been previously linked to GPCR-induced HSP27 phosphorylation in endothelial cells.

To determine whether MK2 was required for thrombin-induced HSP27 phosphorylation, HUVECs were pretreated with or without PF3644022, a specific MK2 inhibitor, stimulated with thrombin over a 60-min time course, and then examined for HSP27 phosphorylation. Thrombin-stimulated phosphorylation of HSP27 at Ser[15] and Ser[78] was significantly attenuated by the MK2 inhibitor PF3644022 compared to that in DMSO-treated control cells (Fig. 4A, lanes 1 to 6 versus lanes 7 to 12). However, thrombin-stimulated phosphorylation of HSP27 at Ser[82] was not altered in the presence of PF3644022 (Fig. 4A, lanes 1 to 6 versus lanes 7 to 12). Thrombin also induced MK2 phosphorylation at Thr[334], a p38 target site, in both control and PF3644022-treated cells (Fig. 4A), indicating that p38 activity was not comprised. Next, siRNA-mediated depletion of MK2 was used to further interrogate MK2 function in thrombin-induced HSP27 phosphorylation. Similar to the effects of PF3644022, thrombin-stimulated phosphorylation of HSP27 at Ser[15] and Ser[78] was significantly inhibited in MK2-depleted cells compared to that in cells transfected with nonspecific siRNA (fig. S4B, lanes 1 to 6 versus lanes 7 to 12). Unlike in the experiments with the PF364422 inhibitor, however, thrombin-induced phosphorylation of HSP27 at Ser[82] was modestly yet significantly decreased at 60 min in MK2-depleted cells (fig. S4B). This discrepancy may be due to the ~75% reduction in p38 protein abundance observed in MK2-depleted cells compared to that in control cells (fig. S4C), which is consistent with previous reports showing that ablation of MK2 protein results in a concomitant reduction in p38 abundance (*23*).

To determine whether HSP27 served as a direct substrate for MK2 in endothelial cells, an in vitro MK2 kinase assay was performed with purified HSP27 as substrate. HUVECs pretreated with or without PF3644022 were incubated with thrombin for 5 min, and endogenous MK2 was immunoprecipitated. MK2 immunoprecipitates were then incubated with purified recombinant glutathione *S*-transferase (GST)–tagged HSP27 and adenosine 5′-triphosphate (ATP) in vitro, and phosphorylation was detected by immunoblotting. MK2 immunoprecipitates from control cells stimulated with thrombin for 5 min showed increases in HSP27 phosphorylation at both Ser[78] and Ser[82] (Fig. 4B, lanes 1 to 3). However, only thrombin-induced HSP27 phosphorylation at Ser[78] was significantly inhibited in cells treated with the MK2 inhibitor PF3644022 (Fig. 4B, lanes 4 to 6), whereas phosphorylation at Ser[82] remained intact. Together, the results from studies of thrombin-stimulated HSP27 phosphorylation in cells and in vitro kinase assays suggest that the phosphorylation of both Ser[78] and Ser[15] requires MK2 activation, whereas the phosphorylation of Ser[82] occurs independently of MK2. These findings further suggest that another kinase present in the MK2 immunoprecipitates is competent to phosphorylate HSP27 at Ser[82].

To examine the function of MK3 in thrombin-induced HSP27 phosphorylation in HUVECs, an MK3 siRNA-targeted depletion approach was used because there are no specific MK3 inhibitors. Endothelial cells transfected with MK3-specific or nonspecific siRNA were stimulated with thrombin over a 30-min time course, and phosphorylation of HSP27 was detected. Thrombin induced significant changes in HSP27 phosphorylation in HUVECs treated with nonspecific siRNA (Fig. 4C, lanes 1 to 4). However, in cells depleted of MK3, only thrombin-stimulated Ser[82] phosphorylation showed a significant decrease at 10 min, whereas there was no significant change
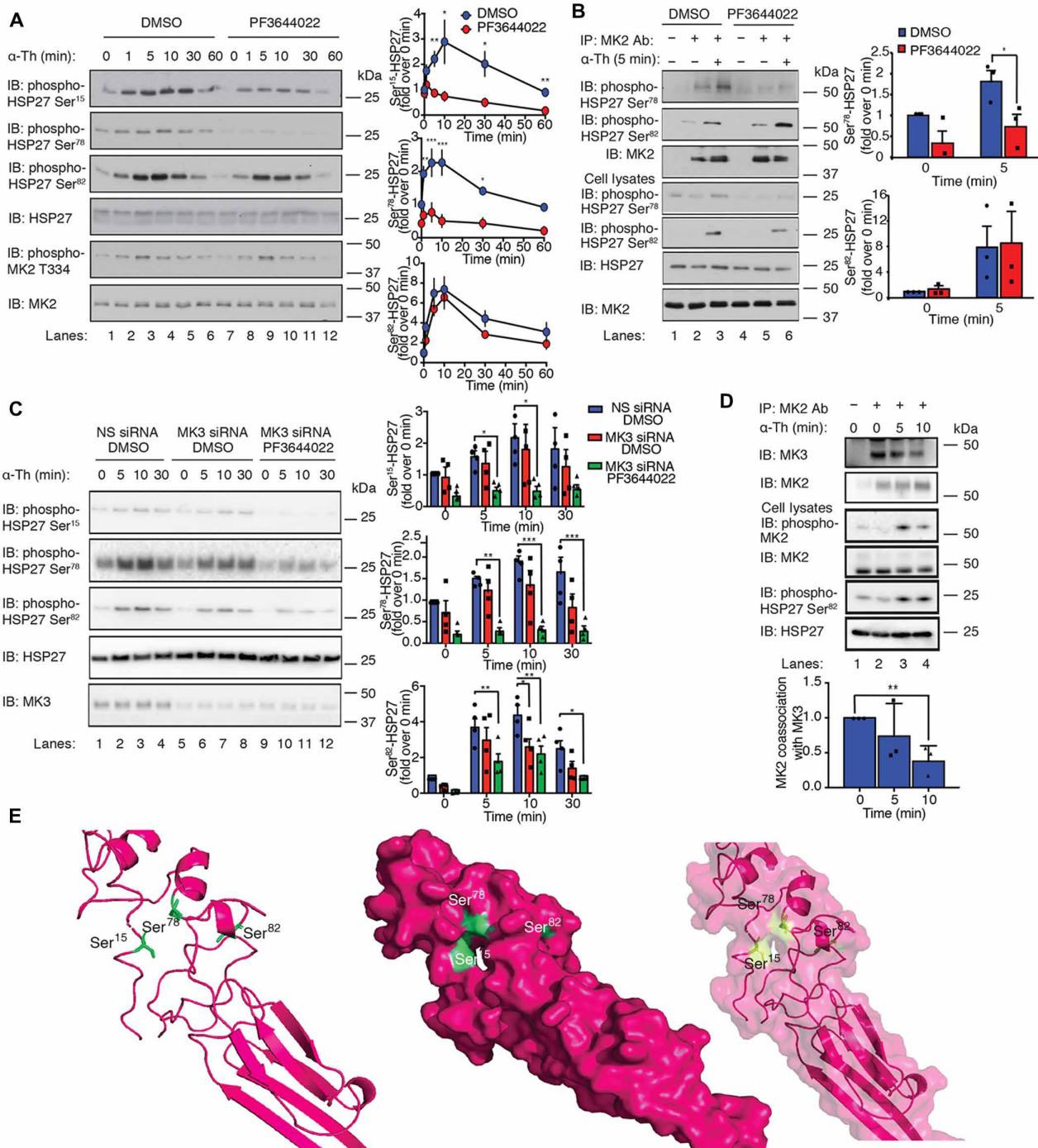
Fig. 4. MK2 and MK3 are required for thrombin-induced HSP27 phosphorylation. (**A**) Left: Immunoblotting analysis of HSP27 and MK2 phosphorylation in HUVECs pretreated with 300 nM PF3644022 (MK2 inhibitor) or DMSO for 1 hour and stimulated with 10 nM thrombin (α-Th) for the indicated times. Blots are representative of four independent experiments. Right: Densitometric analysis of the fold change in the relative abundances of the indicated phosphorylated proteins over time. Data are means ± SD of four independent experiments and were analyzed by Student's *t* test. *$P < 0.05$; **$P < 0.01$; ***$P < 0.001$. (**B**) Left: In vitro assay of MK2 kinase activity. Immuno-blot of HSP27 phosphorylation in HUVECs pretreated with PF3644022 or DMSO and stimulated with 10 nM α-Th. Cell lysates were analyzed by immunoblotting for HSP27 phosphorylation and MK2. Right: Data are means ± SD of four independent experiments and were analyzed by Student's *t* test. *$P < 0.05$. (**C**) Left: Immunoblotting analysis of HSP27 phosphorylation in HUVECs transfected with MK3-specific or nonspecific (NS) siRNAs, pretreated with PF3644022 or DMSO, and stimulated with α-Th. Right: Den-sitometric analysis of the fold change in the relative abundances of the indicated phosphorylated proteins over time. Data are means ± SD of four independent experiments and were analyzed by two-way ANOVA and Dunnett's posttests. *$P < 0.05$; **$P < 0.01$; ***$P < 0.001$. (**D**) Top: Immunoblotting analysis of MK2-MK3 coimmunoprecipitates from HUVECs stimulated with α-Th. Blots of HSP27 and MK2 phosphorylation are representative of three independent experiments. Bottom: Data are means ± SD of three independent experiments and were analyzed by Student's *t* test. **$P < 0.01$. (**E**) Phyre homology modeling of HSP27 residues Ser[15], Ser[78], and Ser[82] within the predicted 3D structure. The three key serine residues are shown in green, and their positions are illustrated in ribbon (left), space-filled (middle), and merged (right) models.

in Ser[15] and Ser[78] phosphorylation (Fig. 4C, lanes 5 to 8). To determine whether MK2 and MK3 were both required to fully phosphorylate HSP27 at these three sites, cells were treated with the MK2 inhibitor PF3644022 and transfected with MK3-specific siRNA. This combination of treatments effectively abolished thrombin-induced HSP27 phosphorylation at all three phosphorylation sites (Fig. 4C, lanes 1 to 4 versus lanes 9 to 12). These results indicate that thrombin-induced HSP27 phosphorylation is differentially regulated, such that MK2 mediates Ser[15] and Ser[78] phosphorylation and MK2 and MK3 are both required for Ser[82] phosphorylation, suggesting a complex regulation of Ser[82] phosphorylation by MK2 and MK3.

MK2 and MK3 form a complex with p38α MAPK, a key upstream kinase activator (24). However, it is not known whether MK2 and MK3 coassociate in endothelial cells and whether thrombin alters this interaction. HUVECs were left unstimulated or were stimulated with thrombin over a 10-min time course, lysed, and immunoprecipitated with anti-MK2 antibody, and coassociated MK3 was detected by immunoblotting. We found that MK2 and MK3 coassociated in unstimulated endothelial cells (Fig. 4D, lanes 1 and 2). However, incubation with thrombin for 10 min caused significant disassociation of the MK2-MK3 complex that correlated with increased Ser[82] phosphorylation (Fig. 4D, lanes 2 to 4). These results suggest that the MK2-MK3 complex is dynamically regulated by thrombin in endothelial cells.

The capacity of MK2 to preferentially phosphorylate Ser[15] and Ser[78] but not Ser[82] is unexpected given the close proximity of Ser[78] and Ser[82] in the primary structure of HSP27, suggesting that the residues exist in a different orientation in the tertiary structure of HSP27. A crystal structure of the highly ordered C-terminal α-crystallin domain of HSP27 has been reported (25); however, Ser[15], Ser[78], and Ser[82] reside in a highly disordered region that is not present in the published structure. To predict the location of the Ser[15], Ser[78], and Ser[82] residues relative to each other in a three-dimensional (3D) structure, we used Phyre homology modeling [PDB (Protein Data Bank) 2N3J] (Fig. 4E) (26). The model predicts that the key residues Ser[15] and Ser[78] are more closely localized within a pocket evident in the space-filled model, whereas Ser[82] is predicted to reside in a distinct pocket (Fig. 4E). The predicted locations of Ser[15] and Ser[78] versus Ser[82] may contribute to the preferential phosphorylation of HSP27 Ser[15] and Ser[78] residues by MK2 versus MK3.

GPCR-induced disassembly of HSP27 oligomers requires p38, MK2, and MK3 activities

HSP27 exists as large oligomers that bind to monomeric actin, whereas phosphorylation of HSP27 promotes oligomer disassembly, releases actin, and promotes actin polymerization (9). To gain mechanistic insight into how thrombin-activated PAR1 regulates HSP27 activity, changes in HSP27 oligomerization status were examined by native, nondenaturing polyacrylamide gel electrophoresis. In HUVECs, thrombin induced the disassembly of large oligomeric complexes of HSP27, resulting in the formation of HSP27 small oligomers that appeared as lower bands on the native gel within minutes. HSP27 large oligomer disassembly with the formation of small oligomers peaked at 10 min after thrombin stimulation, whereas reassembly back into HSP27 larger oligomers occurred by 30 min (Fig. 5A, lanes
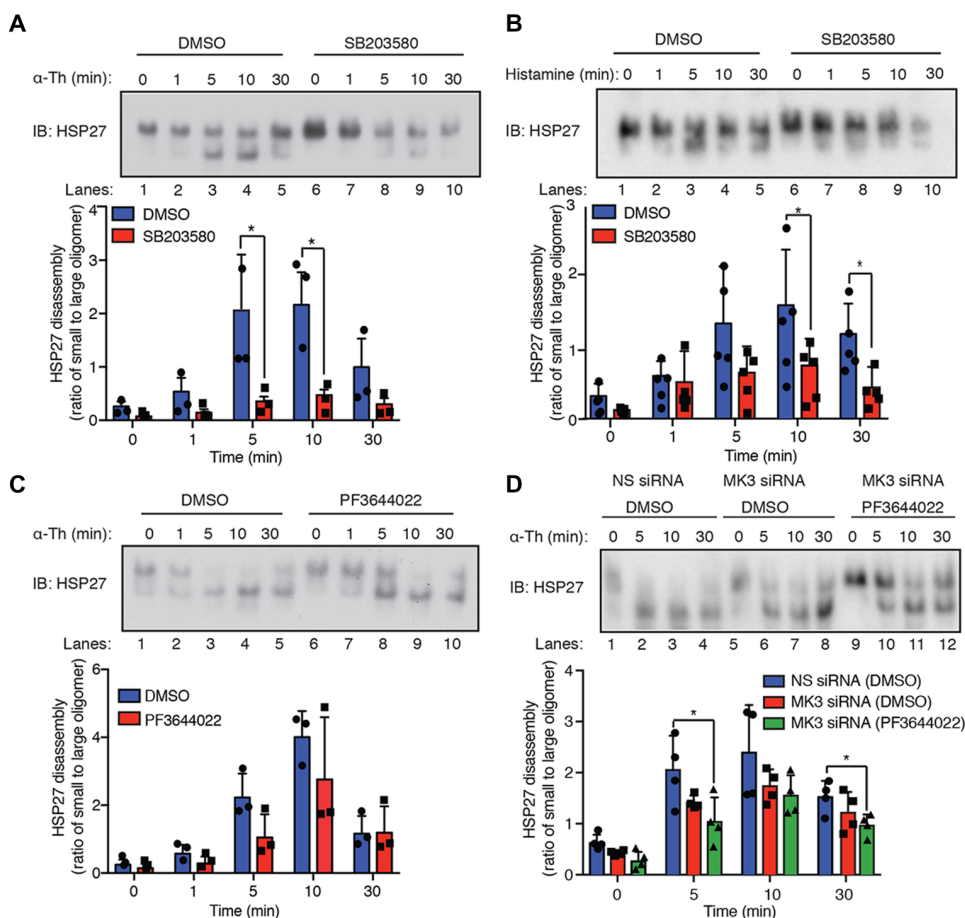

Fig. 5. GPCR-induced HSP27 activity requires p38, MK2, and MK3. (A and **B**) Top: Immunoblotting analysis of HSP27 large oligomer disassembly and reassembly in HUVECs pretreated with 3 μM SB203580 or DMSO for 1 hour and stimulated with (A) 10 nM thrombin (α-Th) or (B) 10 μM histamine and resolved on a native, nondenaturing gel. Blots are representative of three independent experiments. Bottom: Densitometric analysis of the ratio of small to large HSP27 oligomers over time. Data are means ± SD of three (thrombin) or five (histamine) independent experiments and were analyzed by Student's *t* test. *$P < 0.05$. (**C**) Top: Immunoblotting analysis of HSP27 oligomerization in HUVECs pretreated with 300 nM PF3644022 or DMSO for 1 hour and then stimulated with α-Th. Bottom: Data are means ± SD of three independent experiments and were analyzed by Student's *t* test (not significant). (**D**) Top: Immunoblotting analysis of HSP27 oligomerization in HUVECs transfected with MK3-specific or nonspecific (NS) siRNAs, pretreated with PF3644022 or DMSO, and then stimulated with α-Th. Blots are representative of four independent experiments. Bottom: Data are means ± SD of four independent experiments and were analyzed by two-way ANOVA with Dunnett's posttests. *$P < 0.05$.

1 to 5). However, in cells pretreated with the p38 inhibitor SB203580, thrombin-stimulated disassembly of HSP27 larger oligomers was significantly inhibited (Fig. 5A, lanes 6 to 10), indicating that p38 regulates HSP27 disassembly. Histamine also caused the disassembly of HSP27 large oligomers with the resulting formation of small oligomers (Fig. 5B, lanes 1 to 5), which was blocked by SB203580 (Fig. 5B, lanes 6 to 10). These findings indicate that more than one endothelial GPCR regulates HSP27 activity through the p38-dependent modulation of HSP27 large oligomer disassembly.

To determine whether the disassembly of large oligomeric complexes of HSP27 required MK2 function, HUVECs were pretreated with the MK2 inhibitor PF3644022 before being stimulated with thrombin. Inhibition of MK2 failed to block the thrombin-induced disassembly of HSP27 large oligomers, which peaked at 10 min, or the reassembly of HSP27 oligomers at 30 min (Fig. 5C, lanes 1 to 5 versus lanes 6 to 10). Similarly, depletion of MK3 by siRNA failed to inhibit the disassembly of HSP27 large oligomers induced by thrombin or oligomer reassembly compared to that in cells transfected with nonspecific siRNA (Fig. 5D, lanes 1 to 4 versus lanes 5 to 8). These findings indicate that neither MK2 nor MK3 function alone is sufficient to mediate HSP27 oligomer disassembly or reassembly after thrombin stimulation. However, inhibition of both MK2 and MK3 with the combination of PF3644022 and MK3-specific siRNAs caused a significant decrease in thrombin-induced HSP27 oligomer disassembly, where a greater amount of HSP27 large oligomers were detected after 5 min compared to that in control cells treated with DMSO and nonspecific siRNA (Fig. 5D, lanes 2 and 6 versus lane 10). Moreover, inhibition of MK2 and MK3 appeared to enhance the reassembly of large oligomer of HSP27 from the population of small oligomers at 30 min after thrombin stimulation compared to that in control cells (Fig. 5D, lanes 4 and 8 versus lane 12). Together, these findings suggest that the p38-MK2-MK3 signaling axis is required for HSP27 phosphorylation at the Ser[15], Ser[78], and Ser[82] sites, which regulates the dynamics of HSP27 large oligomer disassembly and reassembly after GPCR stimulation.

HSP27 phosphorylation is required for proper endothelial barrier dynamics

Our results indicate that thrombin signaling through the p38-MK2-MK3 axis regulates HSP27 large oligomer disassembly through phosphorylation at three critical sites Ser[15], Ser[78], and Ser[82]. To determine the effect of HSP27 phosphorylation on thrombin-induced endothelial barrier disruption, a siRNA knockdown-rescue approach was taken with siRNA-resistant wild-type HSP27 and a phosphorylation-deficient mutant in which Ser[15], Ser[78], and Ser[82] were converted to alanine (A),

termed triple alanine (TriA) (Fig. 6A). Endogenous HSP27 was detected in cells transfected with nonspecific siRNA coexpressing green fluorescent protein (GFP) and was depleted in GFP-expressing cells transfected with HSP27-specific siRNA (Fig. 6B, lane 1 versus lane 2). Exogenous expression of siRNA-resistant, FLAG-tagged wild type and TriA HSP27 was retained in cells cotransfected with HSP27-specific siRNAs (Fig. 6B, lanes 2 to 4). Exogenous wild type and TriA HSP27 exhibited a slight mobility shift compared to that of endogenous HSP27, which was likely due to the presence of the FLAG epitope (Fig. 6B, lanes 3 and 4 versus lane 1).

We next assessed the effect of phosphorylation on thrombin-induced HSP27 oligomer disassembly in HUVECs by native nondenaturing polyacrylamide gel electrophoresis. Similarly to its regulation of endogenous HSP27, thrombin initiated the disassembly of exogenously expressed wild-type HSP27 large oligomers, which resolved as smaller oligomeric complexes after thrombin stimulation (Fig. 6C, lanes 1 to 3). In contrast, thrombin failed to induce changes in the oligomerization of the HSP27 TriA phosphorylation-deficient mutant (Fig. 6C, lanes 4 to 6). These data suggest that HSP27 phosphorylation at the critical Ser[15], Ser[78], and Ser[82] sites is required to alter HSP27 oligomerization in response to thrombin.

The effect of HSP27 phosphorylation on thrombin-induced endothelial barrier function was next determined by ECIS and a knockdown-rescue
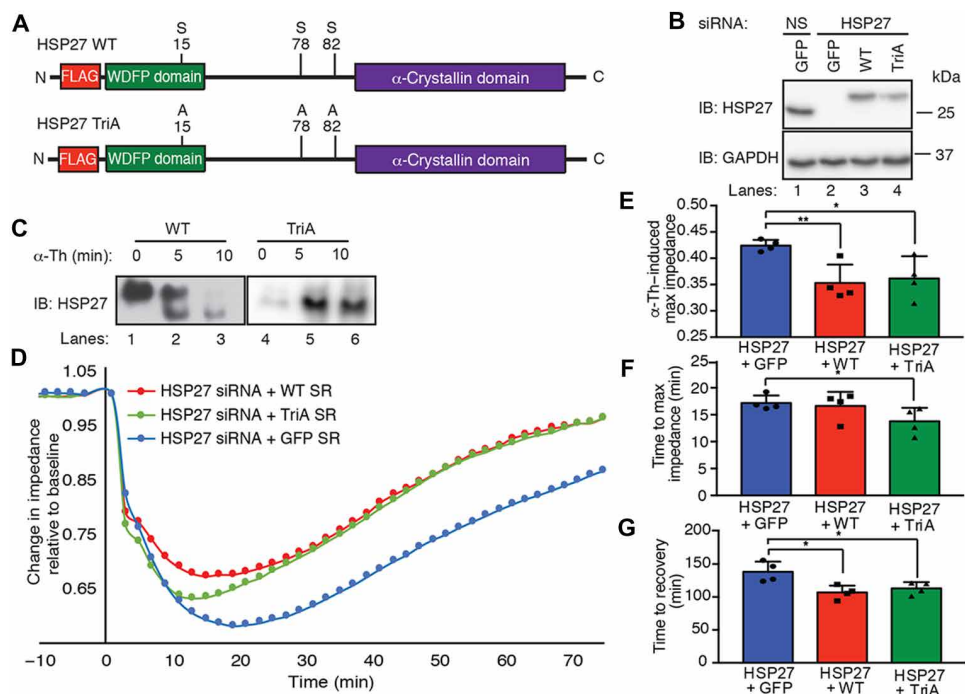

Fig. 6. HSP27 phosphorylation induced by GPCRs regulates endothelial barrier recovery. (**A**) Schematic of N-terminal FLAG-tagged WT HSP27 (*42*) and the HSP27 triple alanine (TriA) mutant. (**B**) Immunoblotting analysis of endogenous and exogenous HSP27 in HeLa cells transfected with HSP27-specific or nonspecific (NS) siRNAs and expressing GFP, siRNA-resistant HSP27 WT, or siRNA-resistant HSP27 TriA mutant. Cell lysates were immunoblotted for GAPDH. (**C**) Immunoblotting analysis of HSP27 WT and TriA oligomerization in HUVECs stimulated with 10 nM thrombin (α-Th) and then resolved on a native, nondenaturing gel. (**D** to **G**) Endothelial barrier impedance or function in HDMECs transfected with HSP27-specific siRNA and re-expressing GFP, siRNA-resistant (*43*) HSP27 WT, or siRNA-resistant HSP27 TriA mutant and stimulated with α-Th, as measured by ECIS (D). The data were normalized to baseline for each condition, and the maximum (max) α-Th–induced change in impedance (E), time to max impedance (F), and time to barrier recovery (G) were quantified from four independent experiments, each performed in duplicate. Data are means ± SEM of four independent experiments and were analyzed by two-way ANOVA and Dunnett's post-tests. *$P < 0.05$; **$P < 0.01$.
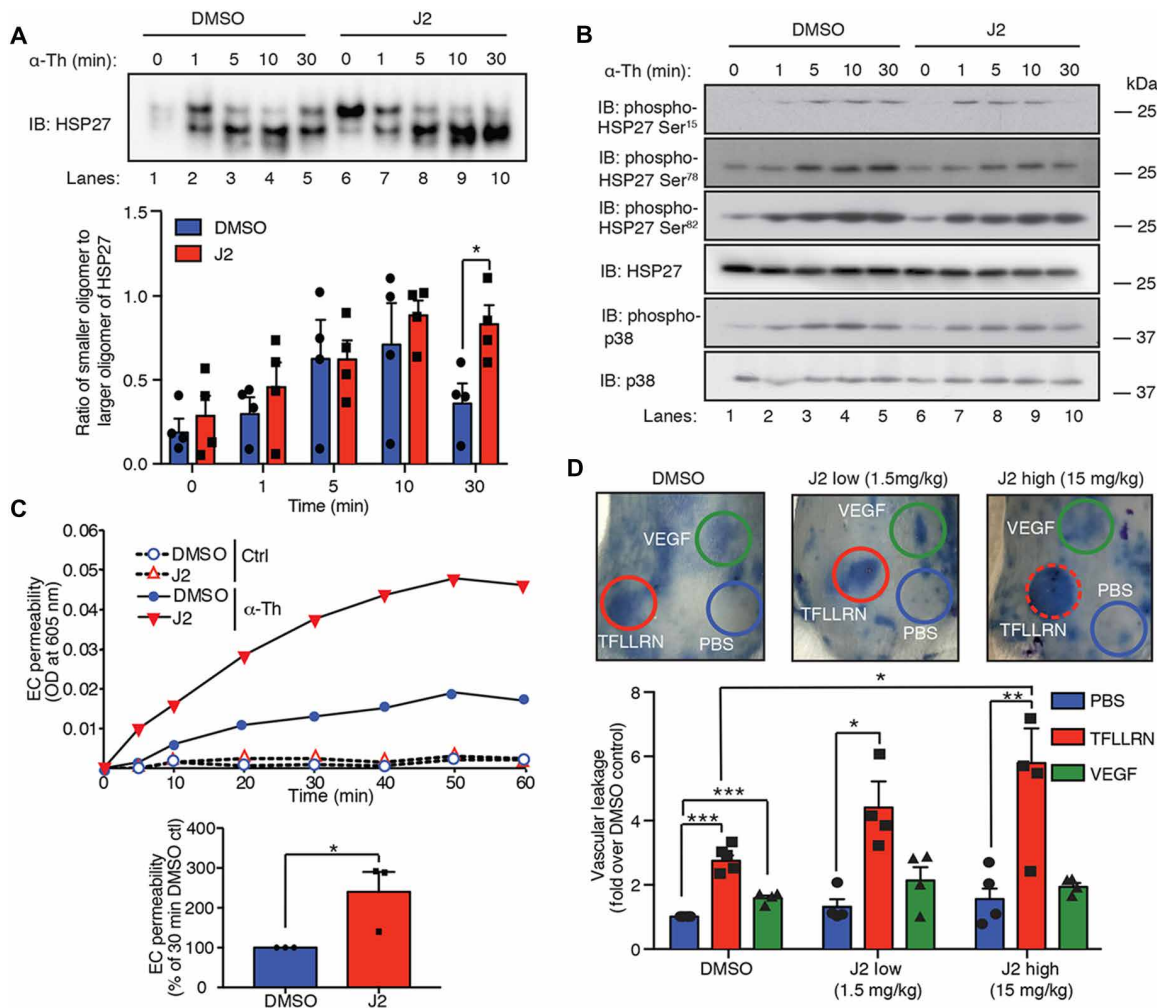
Fig. 7. J2 alters HSP27 oligomerization and PAR1-induced barrier disruption in vitro and enhances vascular leakage in vivo. (**A**) Immunoblotting analysis of HSP27 oligomerization in HUVECs pretreated with the HSP27-specific inhibitor J2 (10 μM) or DMSO for 16 hours and then stimulated with 10 nM thrombin (α-Th). Top: Samples were resolved on a native, nondenaturing gel. Blots are representative of three independent experiments. Bottom: Data are means ± SD of three independent experiments and were analyzed by Student's *t* test. *P < 0.05. (**B**) Immunoblotting analysis of HSP27 and p38 phosphorylation in HUVECs pretreated with J2 or DMSO and then stimulated with α-Th for the indicated times. (**C**) Top: EC barrier permeability was determined by measurement of Evans blue albumin diffusion for HUVECs pretreated with J2 or DMSO and then stimulated with or without α-Th. α-Th–induced EC permeability was quantified at 30 min. Bottom: Data are means ± SD of three independent experiments and were analyzed by Student's *t* test. *P < 0.05. (**D**) Top: Vascular leakage was examined in mice treated with the indicated low or high doses of J2 or DMSO for 16 hours before being injected with PBS, VEGF (4 ng/μl), or TFLLRN (1 μg/μl). Data are means ± SEM of 24 mice from four independent experiments and were analyzed by two-way ANOVA with Dunnett's posttests. *P < 0.05; **P < 0.01; ***P < 0.001.

approach with siRNA-resistant wild type and TriA mutant HSP27 expressed in HDMECs. HDMECs devoid of endogenous HSP27 were electroporated with siRNA-resistant HSP27 wild type or TriA mutant or GFP as a control and then stimulated with thrombin. Under all transfection conditions, the baseline impedance of unstimulated cells was not altered (Fig. 6D). Thrombin-initiated rapid barrier disruption also remained intact (Fig. 6D), suggesting that HSP27 was not required for the initiation of barrier disruption. However, in HDMECs coexpressing GFP, depletion of endogenous HSP27 enhanced the thrombin-induced maximal impedance and slowed barrier recovery (Fig. 6, D to G), similarly to that observed in earlier experiments (Fig. 3, C and D). Expression of siRNA-resistant wild-type HSP27 in

HDMECs lacking endogenous HSP27 restored most aspects of barrier function by significantly reducing thrombin induced maximal impedance and recovery time (Fig. 6, D, E, and G). A similar effect was observed in HDMECs expressing the siRNA-resistant HSP27 phosphorylation-deficient TriA mutant (Fig. 6, D, E and G). However, expression of the TriA mutant significantly decreased the time to maximal impedance compared to that in cells expressing wild-type HSP27 (Fig. 6, D and F), suggesting that HSP27 dephosphorylation may be required for efficient endothelial barrier recovery. These data suggest that the thrombin-induced, p38-MK2-MK3–mediated phosphorylation of HSP27 controls the dynamics of HSP27 oligomer disassembly and reassembly to properly regulate endothelial barrier recovery.

Disruption of HSP27 oligomerization enhances PAR1-induced endothelial barrier permeability in vitro and vascular leakage in vivo

Next, we determined the role of HSP27 oligomerization on PAR1-induced endothelial barrier function in vitro and in vivo in experiments with J2, a specific inhibitor of HSP27. J2 promotes HSP27 cross-linking, alters dimer formation, and results in functional inhibition of HSP27 activity (27). To determine the effects of J2 on HSP27 oligomerization, HUVECs were pretreated with J2 and then stimulated with thrombin. J2 failed to block thrombin-induced HSP27 oligomer disassembly compared to that in DMSO-treated control treated cells (Fig. 6A, lanes 1 to 4 versus lanes 6 to 9). However, J2 treatment significantly inhibited reassembly of HSP27 large oligomer complexes after 30 min of thrombin stimulation compared to that in control cells (Fig. 7A, lane 5 versus lane 10). The effect of J2 on HSP27 large oligomer reassembly was not due to alterations in phosphorylation, because J2 failed to block thrombin-induced HSP27 phosphorylation at Ser^{15}, Ser^{78}, and Ser^{82} (Fig. 7B, lanes 1 to 5 versus lanes 6 to 10). Thus, J2 altered the dynamics of reassembly of large HSP27 oligomers after their thrombin-stimulated disassembly.

To assess the effect of altered HSP27 oligomer reassembly on PAR1-induced endothelial permeability, HUVECs were treated with or without J2, stimulated with thrombin, and the flux of Evans blue–bound albumin was quantified. J2 did not alter baseline permeability compared to that of DMSO-treated control cells (Fig. 7C). However, HUVECs treated with J2 exhibited a significant increase in thrombin-induced endothelial permeability at 30 min compared to that of control cells (Fig. 7C), similar to that observed in experiments with HSP27-depleted cells (Fig. 3, A and B). Together, these results suggest that the proper dynamics of HSP27 oligomer disassembly and reassembly has a critical function in controlling endothelial barrier recovery after PAR1 activation.

To determine whether the altered reassembly of HSP27 oligomers affected PAR1-induced vascular leakage in vivo, we treated mice with or without J2 and then measured vascular leakage with the Miles assay (4). In these studies, the PAR1-specific synthetic peptide TFLLRN rather than thrombin was used to activate endothelial PAR1, because thrombin activates the murine platelet receptor PAR4, which results in activation and aggregation (28). PAR1 is not expressed in murine platelets. Mice were pretreated with J2 at either a high (15 mg/ml) or low (1.5 mg/ml) dose and then stimulated with TFLLRN, vascular endothelial growth factor (VEGF), or phosphate-buffered saline (PBS) before vascular leakage was measured. Under control conditions, basal vascular leakage was not altered by J2 compared to that in DMSO-treated control mice (Fig. 7D). Intradermal injections of the PAR1-specific peptide agonist, TFLLRN, induced a marked increase in Evans blue–bound albumin leakage compared to that in the DMSO-treated control mice injected with PBS (Fig. 7D). However, vascular leakage induced by the TFLLRN-dependent activation of PAR1 was significantly enhanced in mice pretreated with J2 (Fig. 7D), consistent with the enhanced thrombin-induced barrier permeability that we observed in HSP27-depleted endothelial cells in vitro (Figs. 3A and 6D). Unlike for PAR1-stimulated vascular leakage, inhibition of HSP27 by J2 failed to affect VEGF-induced vascular leakage (Fig. 7D), indicating that the effect of HSP27 activity on barrier function was specific to PAR1, a mediator of proinflammatory responses. Together, these results suggest that HSP27 has a critical role in regulating activated PAR1-induced endothelial barrier permeability in vitro and in vivo.

DISCUSSION

The intracellular signaling pathways induced by GPCRs that control the dynamics of endothelial barrier disruption and recovery remain poorly defined. In this study, we identified a GPCR-induced p38-dependent MK2-MK3 inflammatory signaling pathway that mediated HSP27 phosphorylation and activation, which functions to control endothelial barrier recovery (Fig. 8). We showed that GPCR-induced phosphorylation of HSP27 was dependent on the p38-MK2-MK3 signaling axis and was critical for proper HSP27 oligomer disassembly and reassembly and endothelial barrier recovery in vitro. We further demonstrated that HSP27 regulated vascular leakage in response to PAR1 activation in vivo. Together, these data provide mechanistic understanding of HSP27 function in endothelial barrier recovery after stimulation with proinflammatory GPCR agonists.

We showed that thrombin stimulated HSP27 phosphorylation in different endothelial cell types, whereas previous reports showed thrombin-induced HSP27 phosphorylation in vascular smooth muscle cells and platelets (29, 30). However, our study provides mechanistic insight, demonstrating that the thrombin-dependent activation of PAR1-induced HSP27 phosphorylation was mediated by the p38 effectors MK2 and MK3 through a pathway independent of the canonical RhoA and MLC pathway, which promotes endothelial barrier disruption. Moreover, the p38-MK2-MK3 signaling pathway displayed a slower onset, peaking between 5 and 10 min, compared to the rapid activation of RhoA and MLC phosphorylation induced by thrombin, which occurs within 1 to 2 min (Fig. 1), suggesting that these temporally distinct signaling pathways may impart different functions on endothelial barrier regulation. We also defined four different combinations of HSP27 phosphorylation sites induced by thrombin in endothelial cells by mass spectrometry (MS; Fig. 1, C and D). Whereas Ser^{82} and Ser^{15} appeared to be phosphorylated alone, Ser^{78} phosphorylation was only detected in combination with that of Ser^{82} or Ser^{83}, suggesting that there may be a specific order in which HSP27 is phosphorylated at each site in response to thrombin. Two of the HSP27 phosphorylation sites, Ser^{15} and Ser^{82}, were previously identified by MS in endothelial cells stimulated with the PAR1 peptide agonist (31), consistent with our results. In addition to being activated by thrombin, we showed that p38-MK2-MK3–mediated HSP27 phosphorylation and activation was induced by histamine, indicating that the pathway is activated by other endothelial GPCRs. Bradykinin, an inflammatory mediator that induces vascular permeability (32), is also likely to signal through the p38-MK2-MK3 pathway to regulate HSP27 function and barrier recovery similarly to thrombin and histamine but has yet to be tested. Thus, different endothelial GPCRs induce p38-MK2-MK3 signaling, which displays temporally distinct kinetics compared to those of the RhoA-MLC pathway implicated in barrier disruption.

In this study, we sought to define a link between HSP27 function and GPCR-induced endothelial barrier regulation and found an unexpected role for HSP27 in endothelial barrier recovery. We and others showed that thrombin-activated p38 promotes endothelial barrier permeability but not barrier stabilization (3, 4). However, we found that inhibition of HSP27 function substantially enhanced thrombin-induced barrier permeability in vivo. These findings suggest that HSP27 functions in barrier recovery, rather than in the initiation of barrier disruption, which is consistent with a study showing that HSP27 overexpression enhances blood-brain barrier stabilization (10). The different effects of p38 versus HSP27 on barrier
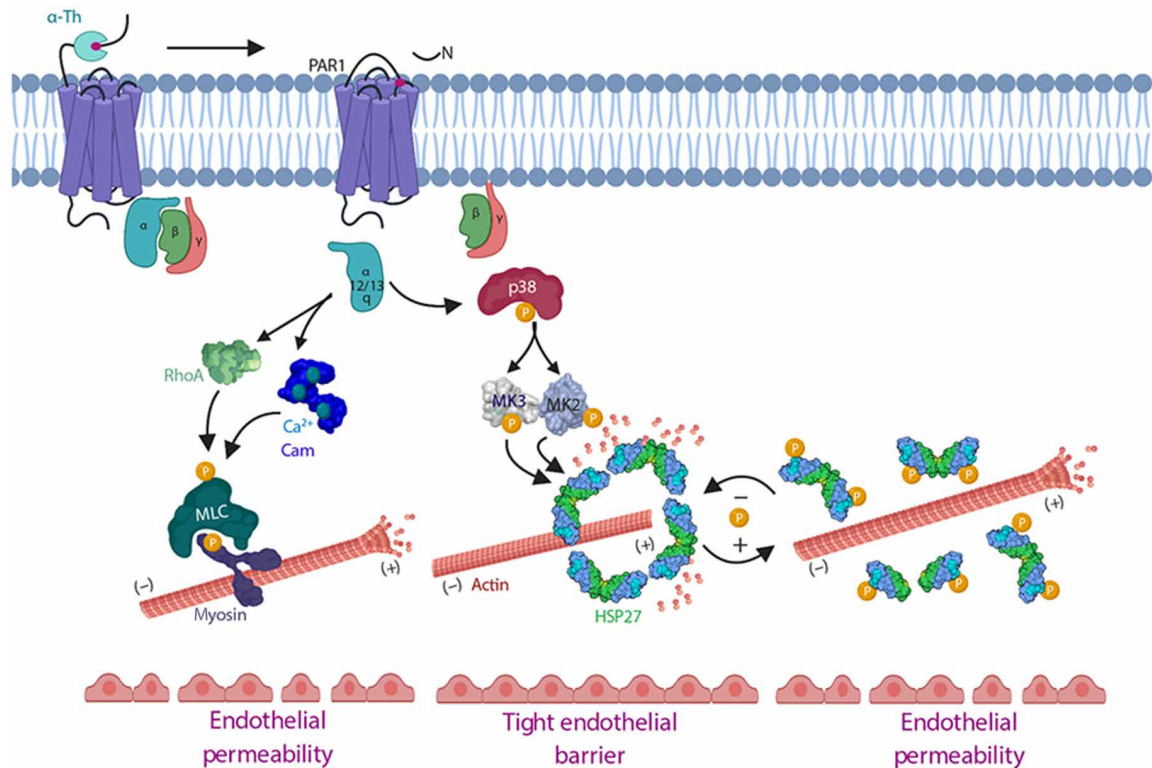
Fig. 8. Model of GPCR-induced p38-MK2-MK3 signaling and the HSP27-mediated regulation of endothelial barrier recovery. Thrombin-activated PAR1 couples to Gα$_q$ and promotes rapid increases in Ca^{2+} binding to calmodulin (Cam), which initiates MLC phosphorylation, actin-myosin contractility, and endothelial barrier permeability. Activated PAR1 also couples to Gα$_{12/13}$ and activates RhoA signaling, which also enhances MLC phosphorylation and endothelial barrier permeability. Here, we showed that thrombin-activated PAR1 initiated a p38-MK2-MK3 signaling pathway that occurred independently of the RhoA-MLC pathway to regulate the phosphorylation and activity of HSP27 to control endothelial barrier recovery. GPCR-induced HSP27 phosphorylation and oligomer disassembly are expected to release actin, promote actin polymerization, and contribute to endothelial barrier disruption, whereas HSP27 dephosphorylation facilitates HSP27 oligomer reassembly and endothelial barrier recovery. Thus, GPCRs activate multiple signaling pathways that promote endothelial barrier disruption and recovery.

integrity are likely due to the broad actions of p38 on multiple downstream effectors (*33*) that modulate adherens junction destabilization (*34*) and actomyosin contractility (*35*). Although thrombin transiently disrupts barrier function through the modulation of adherens junction and actin myosin contractility (*36*, *37*), there is limited knowledge of the mechanisms responsible for recovery of the endothelial barrier. A previous study showed that Gβγ signaling through focal adhesion kinase modulates adherens junction reassembly and recovery of barrier function after thrombin stimulation (*15*). Our study now indicates that regulation of endothelial barrier recovery by thrombin and other proinflammatory GPCR agonists also requires HSP27 function, indicating that barrier recovery, similarly to barrier disruption, is controlled by multiple pathways.

The work presented here also provides mechanistic insight into how p38, MK2, and MK3 signaling regulates HSP27 phosphorylation induced by GPCR activation in a physiologically relevant endothelial cell system. In vitro, MK2 and MK3 both phosphorylate Ser[15], Ser[78], and Ser[82] of HSP27 (*21*, *38*), indicating that MK2 and MK3 may have redundant or compensatory functions (*23*). However, our results suggest that thrombin-activated MK2 signaling specifically phosphorylates HSP27 at Ser[78] and Ser[15], and not Ser[82], whereas thrombin-activated MK3 preferentially phosphorylates HSP27 at Ser[82]. These findings indicate that MK2 and MK3 differentially phosphorylate HSP27 in endothelial cells in response to thrombin. A

plausible explanation for the differential phosphorylation of HSP27 mediated by two different kinases might be related to the different locations of each residue as predicted by Phyre modeling analysis. In addition, MK2 and MK3 exist in a complex that disassociates after thrombin stimulation (Fig. 4D), which may enable the kinases to bind to and phosphorylate specific serine residues in spatially distinct locations.

We further showed that direct modulation of endogenous HSP27 activity through altering the disassembly and reassembly of large HSP27 oligomers was regulated by GPCRs in endothelial cells. Thrombin- and histamine-induced phosphorylation of HSP27 correlated with changes in HSP27 activity. The peak in the phosphorylation and disassembly of HSP27 large oligomers induced by GPCRs occurred between 5 and 10 min after stimulation, whereas HSP27 large oligomer reassembly occurred at ~30 min, a time when HSP27 phosphorylation began to decline (Figs. 2 and 5). The changes in HSP27 peak activity also correlated temporally with the initiation of barrier recovery as observed with ECIS (Figs. 3C and 6D). These findings are consistent with the idea that fine-tuned regulation of HSP27 activity is controlled by phosphorylation and dephosphorylation events, which, in turn, control the appropriate regulation of endothelial barrier recovery. Here, we showed that MK2 and MK3 were primarily responsible for HSP27 phosphorylation and activity. However, neither inhibition of MK2 or MK3 alone was sufficient to block HSP27

oligomer disassembly. In contrast, blockade of MK2 and MK3 together caused partial, but significant, inhibition of disassembly of HSP27 oligomers, although to a lesser extent than that observed when p38 activity was inhibited. In addition to altering HSP27 oligomer disassembly, inhibition of MK2 and MK3 in combination appeared to enhance the reassembly of large oligomeric complexes of HSP27, suggesting a role for HSP27 dephosphorylation. The phosphatase PP2A dephosphorylates HSP27 in vitro (39) but has not been shown to function in the regulation of HSP27 phosphorylation in any cell type.

Last, our results suggest that GPCR-induced HSP27 activity functions primarily to control endothelial barrier recovery. In siRNA knockdown rescue studies, an HSP27 phosphorylation-deficient TriA mutant that lacks the capacity to undergo oligomer disassembly failed to restore the proper dynamics of endothelial barrier recovery compared to wild-type HSP27 in response to thrombin stimulation. In addition, J2 failed to block thrombin-induced HSP27 phosphorylation and large oligomer disassembly but markedly inhibited the reassembly of HSP27 large oligomers and enhanced endothelial barrier permeability in vitro. Consistent with a role for HSP27 in barrier recovery, we showed that treatment of female mice with J2 enhanced vascular leakage induced by the activation of PAR1 but failed to affect VEGF-induced vascular leakage. Note that a previous study using *HSPB1*-null mice (*HSPB1* encodes HSP27) observed sex-selective sensitivity to endothelial nitric oxide synthase inhibition, with female mice exhibiting greater sensitivity than male mice (40). These findings raise the possibility that modulation of vascular leakage observed with J2 may exhibit sex-selective sensitivity, but this has not been tested. In summary, this study provides mechanistic insight into the role of HSP27 in the GPCR-mediated regulation of endothelial barrier recovery in vitro and in vivo.

MATERIALS AND METHODS
Antibodies and reagents
α-Thrombin was purchased from Enzyme Research Laboratories. The murine PAR1 agonist peptide TFLLRN and the human PAR1 agonist peptide TFLLRNPNDK were synthesized and purified by reverse-phase, high-pressure liquid chromatography at Tufts University Core Facility. Histamine dihydrochloride was obtained from Tocris. VEGF was purchased from PeproTech. Rabbit immunoglobulin G antibody and purified GST-HSP27 were obtained from Rockland Immunochemicals. The J2 HSP27 inhibitor was synthesized and purchased from ProbeChem. PF3644022 was purchased from Tocris. SB203580 was from LC Laboratories. Vorapaxar was from Axon MedChem and Fasudil was from LC Laboratories. Polyclonal rabbit anti-p38, polyclonal rabbit anti-MK2, polyclonal rabbit anti-MK3, polyclonal rabbit phospho-MK2 (Thr[334]), polyclonal rabbit anti-MLC, polyclonal rabbit anti-MYPT1, polyclonal rabbit anti–phospho-MYPT1, monoclonal mouse anti–phospho-MLC, monoclonal mouse anti-HSP27, and polyclonal rabbit phospho-HSP27 (Ser[15], Ser[78], and Ser[82]) antibodies were purchased from Cell Signaling Technology. Monoclonal mouse anti–glyceraldehyde-3-phosphate dehydrogenase (GAPDH) antibody was from GeneTex. Monoclonal mouse anti-RhoA antibody was from Santa Cruz Biotechnology. Horseradish peroxidase–conjugated goat–anti-rabbit and goat–anti-mouse antibodies were from Bio-Rad Laboratories.

Cell culture and plasmids
HUVECs and HDMECs were purchased from Lonza and were grown and maintained according to the manufacturer's instructions and used up to passage 6. HUVEC-derived EA.hy926 cells were obtained from the American Type Culture Collection. PAR1-expressing HeLa cells and EA.hy926 cells were grown in Dulbecco's modified Eagle's medium/F12 medium with 10% fetal bovine serum. All cells were cultured in a 37°C incubator with 5% CO_2. N-terminal FLAG-tagged human HSP27 wild type and the TriA mutant in pcDNA3 were provided by G. Brewer (Rutgers University, New Brunswick, NJ). siRNA-resistant HSP27 mutants were generated by QuikChange site-directed mutagenesis (Agilent Technologies) and included five silent point mutations (c387t, g390a, t393c, c396t, and c399t) within the siRNA-targeted region. All HSP27 point mutations were confirmed by dideoxy sequencing.

Mass spectrometry
Thrombin-induced HSP27 phosphorylation in HUVEC-derived EA.hy926 cells was determined in three biological replicates through a tandem mass tag 10-plexed MS quantitative phospho-proteomic analysis as recently described (12). The MS data have been deposited on MassIVE (https://massive.ucsd.edu/ProteoSAFe/static/massive.jsp; dataset identifier: MSV000084604) and on the ProteomeXchange (http://proteomecentral.proteomexchange.org/cgi/GetDataset; dataset: PXD016368).

RhoA activity assay
RhoA activity was measured as was previously described (41). Briefly, GST-rhotekin Rho-binding domain (RBD) fusion protein was prepared and purified by standard techniques. After agonist stimulation, EA.hy926 cells were lysed, and equivalent amounts of lysates were used in pull-down assays with GST rhotekin-RBD bound to Glutathione Sepharose beads. RhoA was eluted, resolved by SDS–polyacrylamide gel electrophoresis (PAGE), transferred to polyvinylidene difluoride (PVDF) membranes, and then analyzed by immunoblotting with anti-RhoA antibody. Immunoblots were developed with enhanced chemiluminescence, and band intensities were analyzed by densitometry.

Immunoblotting
HUVECs, HDMECs, and EA.hy926 endothelial cells were serum-starved for 2 hours and then treated with or without agonists under various conditions. Cells were lysed in 2× SDS Laemmli sample buffer containing 200 mM dithiothreitol (DTT). Equivalent amounts of cell lysates were resolved by SDS-PAGE, transferred to PVDF membranes, and incubated with antibodies specific for the phosphorylated forms of p38, HSP27, MLC, MYPT1, and MK2, as well as with antibodies against p38, HSP27, MLC, MYPT1, MK2, MK3, and p38α. Cell lysates were also analyzed by immunoblotting to detect GAPDH. Membranes were developed by chemiluminescence and band intensities were quantified by densitometry with ImageJ software (National Institutes of Health).

Transfection of cells with siRNA and rescue experiments
HUVECs and HDMECs were transfected with siRNAs using TransIT-X2 (Mirus Bio) according to the manufacturer's instructions. HSPB1-specific (HSP27) siRNA (5′-AAGGACGAGCATGGCTACATC-3′) was used at 12.5 nM in HUVECs and at 25 nM in HDMECs; MK2-specific siRNA (5′-CTACGAGCAGATCAAGATAAA-3′) was used at 25 nM;

MK3-specific siRNA (5′-CCAGATAGTAATAAACACCAT-3′) was used at 25 nM; and MAPK14-specific (p38α) siRNA (5′-AACTGC-GGTTACTTAAACATA-3′) was used at 25 nM. All siRNAs, including nonspecific AllStars Negative Control siRNA (5′-GGCUACGUC-CAGGAGCGCACC-3′), were purchased from Qiagen. HSP27 siRNA knockdown-rescue experiments were performed by transfecting HDMECs with HSP27-specific siRNA or nonspecific siRNA control for 5 days. The siRNA-resistant HSP27 wild type and TriA mutant cDNA plasmids (0.2 μg) were introduced into HDMECs by electroporation and barrier impedance was determined after 36 hours.

Native gel electrophoresis
HUVECs were serum-starved and treated with agonists under various conditions with or without inhibitors, as appropriate. Cells were lysed in 2× Laemmli sample buffer without DTT. Samples were resolved on native PAGE gels in nondenaturing running buffer (25 mM tris-HCl and 192 mM glycine), transferred to PDVF membranes, and analyzed by immunoblotting with anti-HSP27 antibody. Membranes were developed by chemiluminescence and band intensities were quantified by densitometry.

Immunoprecipitation and in vitro kinase assay
HUVECs were grown in 6-cm dishes for 3 days, serum-starved for 2 hours, treated with or without thrombin, and lysed in Triton X-100 lysis buffer [200 mM tris-HCl (pH 7.0), 1.5 mM NaCl, 10% Triton X-100, 10 mM EDTA, 10 mM EGTA, 10 mM β-glycerophosphate, 25 mM NaPP, 10 mM NaVO$_4$, leupeptin (10 μg/ml), aprotinin (10 μg/ml), trypsin protease inhibitor (10 μg/ml), pepstatin (10 μg/ml), and phenylmethylsulfonyl fluoride (10 μg/ml)], as previously described [4]. Cell lysates were homogenized and cleared by centrifugation and equivalent amounts of lysates were used for immunoprecipitations with the anti-MK2 antibody. Samples were eluted with 2× Laemmli sample buffer containing 200 mM DTT, resolved by SDS-PAGE, transferred to PVDF membranes, and developed by chemiluminescence. In vitro kinase assays were performed with immunoprecipitated MK2 in the presence of 200 μM ATP and the purified kinase substrate GST-HSP27 for 30 min at 30°C in kinase buffer containing 250 mM tris-HCl (pH 7.0), 20 mM DTT, 50 mM β-glycerophosphate, 1 mM NaVO$_4$, and 100 mM MgCl$_2$. Samples were eluted in 2× Laemmli sample buffer and resolved by SDS-PAGE. Cell lysates were also analyzed by immunoblotting with specific antibodies as indicated in the figure legends.

Endothelial cell barrier permeability
Endothelial cell barrier permeability was quantified by measuring the flux of Evans blue–bound albumin as previously described [4]. HUVECs were seeded onto collagen-coated 3.0-μm transwell permeability support chambers (Corning) and grown for 5 days until confluent. Cells were serum-starved for 2 hours and then treated with thrombin. Evans blue conjugated to bovine serum albumin (BSA) was added to the upper chamber after 10 or 30 min of thrombin stimulation. Samples were removed from the lower chamber at the times indicated in the figure legends and the amount of Evans blue–BSA diffusion was quantified by measuring the absorbance at 605 nm with a microplate reader (SpectraMax Plus, Molecular Devices).

Electrical cell impedance sensing
HDMECs were seeded onto cysteine- and collagen-coated gold microwell 8W10E+ ECIS array (Applied Biophysics) and allowed to reach confluence for 48 to 72 hours until impedance reached 3000 ohms. The baseline barrier was recorded and established by multiple frequency time. Changes in impedance, a measure of barrier function, was determined after the addition of thrombin and recording continued until the barrier recovered to the previously established baseline impedance.

Vascular leakage assay
Vascular leakage was measured in mice as was previously described with minor modifications [4]. Briefly, 8-week-old CD1/CD1 female mice were injected intraperitoneally with 100 μl of DMSO or 1.5 or 15 mg/kg of the HSP27 inhibitor J2. After 24 hours, mice were anesthetized and were injected in the tail vein with 200 μl of 1.0% Evans blue 0.1% BSA diluted in PBS. After 1 min, 50 μl of 0.1% BSA in PBS, VEGF (4 ng/μl), or TFLLRN peptide (1 μg/μl) were injected intradermally into separate areas of the shaved back skin of the mouse. The mice were euthanized 10 min after injection, and an 8-mm punch biopsy of skin containing the site of injection was removed. The skin biopsies were incubated in 500 μl of formamide at 65°C for 24 hours, and the amount of extracted Evans blue dye was measured with a microplate reader at optical density at 595 nm. Animal studies were performed in accordance with the recommendations in the Guide for the Care and Use of Laboratory Animals of the National Institutes of Health under protocols approved by the Institutional Animal Care and Use Committee at the University of California, San Diego.

Models and prediction analysis
Schematics were created in Adobe Illustrator. The model in Fig. 8 was generated with BioRender.com. The Phyre^2 web portal (http://www.sbg.bio.ic.ac.uk/~phyre2/html/page.cgi?id=index) was used for HSP27 protein prediction modeling [26]. PHOXTRACK software was used to predict causal kinases [17].

Statistical analysis
Data were analyzed with Prism 7.0 statistical software, Microsoft Excel, R, and Morpheus (https://software.broadinstitute.org/morpheus/). Statistical analysis methods are indicated in the figure legends.

REFERENCES AND NOTES

1. Y. Komarova, A. B. Malik, Regulation of endothelial permeability via paracellular and transcellular transport pathways. *Annu. Rev. Physiol.* **72**, 463–493 (2010).
2. L. Sun, R. D. Ye, Role of G protein-coupled receptors in inflammation. *Acta Pharmacol. Sin.* **33**, 342–350 (2012).
3. T. Borbiev, A. Birukova, F. Liu, S. Nurmukhambetova, W. T. Gerthoffer, J. G. Garcia, A. D. Verin, p38 MAP kinase-dependent regulation of endothelial cell permeability. *Am. J. Physiol. Lung Cell. Mol. Physiol.* **287**, L911–L918 (2004).
4. N. J. Grimsey, B. Aguilar, T. H. Smith, P. Le, A. L. Soohoo, M. A. Puthenveedu, V. Nizet, J. Trejo, Ubiquitin plays an atypical role in GPCR-induced p38 MAP kinase activation on endosomes. *J. Cell Biol.* **210**, 1117–1131 (2015).
5. N. J. Grimsey, Y. Lin, R. Narala, C. C. Rada, H. Mejia-Pena, J. Trejo, G protein-coupled receptors activate p38 MAPK via a non-canonical TAB1-TAB2- and TAB1-TAB3-dependent pathway in endothelial cells. *J. Biol. Chem.* **294**, 5867–5878 (2019).
6. S. P. Adderley, X. E. Zhang, J. W. Breslin, Involvement of the H1 histamine receptor, p38 MAP kinase, myosin light chains kinase, and Rho/ROCK in histamine-induced endothelial barrier dysfunction. *Microcirculation* **22**, 237–248 (2015).

7. S. Pichon, M. Bryckaert, E. Berrou, Control of actin dynamics by p38 MAP kinase - Hsp27 distribution in the lamellipodium of smooth muscle cells. *J. Cell Sci.* **117**, 2569–2577 (2004).

8. T. Rogalla, M. Ehrnsperger, X. Preville, A. Kotlyarov, G. Lutsch, C. Ducasse, C. Paul, M. Wieske, A. P. Arrigo, J. Buchner, M. Gaestel, Regulation of Hsp27 oligomerization, chaperone function, and protective activity against oxidative stress/tumor necrosis factor α by phosphorylation. *J. Biol. Chem.* **274**, 18947–18956 (1999).

9. S. Salinthone, M. Tyagi, W. T. Gerthoffer, Small heat shock proteins in smooth muscle. *Pharmacol. Ther.* **119**, 44–54 (2008).

10. Y. Shi, X. Jiang, L. Zhang, H. Pu, X. Hu, W. Zhang, W. Cai, Y. Gao, R. K. Leak, R. F. Keep, M. V. Bennett, J. Chen, Endothelium-targeted overexpression of heat shock protein 27 ameliorates blood-brain barrier disruption after ischemic brain injury. *Proc. Natl. Acad. Sci. U.S.A.* **114**, E1243–E1252 (2017).

11. S. Kostenko, U. Moens, Heat shock protein 27 phosphorylation: Kinases, phosphatases, functions and pathology. *Cell. Mol. Life Sci.* **66**, 3289–3307 (2009).

12. Y. Lin, J. M. Wozniak, N. J. Grimsey, S. Girada, A. Patwardhan, O. Molinar-Inglis, T. H. Smith, J. D. Lapek, D. J. Gonzalez, J. Trejo, Phosphoproteomic analysis of protease-activated receptor-1 biased signaling reveals unique modulators of endothelial barrier function. *Proc. Natl. Acad. Sci. U.S.A.* **117**, 5039–5048 (2020).

13. H. B. Sun, X. Ren, J. Liu, X. W. Guo, X. P. Jiang, D. X. Zhang, Y. S. Huang, J. P. Zhang, HSP27 phosphorylation protects against endothelial barrier dysfunction under burn serum challenge. *Biochem. Biophys. Res. Commun.* **463**, 377–383 (2015).

14. X. Sun, Y. Yin, L. Kong, W. Chen, C. Miao, J. Chen, The effect of propofol on hypoxia-modulated expression of heat shock proteins: Potential mechanism in modulating blood-brain barrier permeability. *Mol. Cell. Biochem.* **462**, 85–96 (2019).

15. N. Knezevic, M. Tauseef, T. Thennes, D. Mehta, The G protein betagamma subunit mediates reannealing of adherens junctions to reverse endothelial permeability increase by thrombin. *J. Exp. Med.* **206**, 2761–2777 (2009).

16. N. J. Grimsey, R. Narala, C. C. Rada, S. Mehta, B. S. Stephens, I. Kufareva, J. Lapek, D. J. Gonzalez, T. M. Handel, J. Zhang, J. Trejo, A tyrosine switch on NEDD4-2 E3 ligase transmits GPCR inflammatory signaling. *Cell Rep.* **24**, 3312–3323.e5 (2018).

17. C. Weidner, C. Fischer, S. Sauer, PHOXTRACK-a tool for interpreting comprehensive datasets of post-translational modifications of proteins. *Bioinformatics* **30**, 3410–3411 (2014).

18. M. van den Biggelaar, J. R. Hernandez-Fernaud, B. L. van den Eshof, L. J. Neilson, A. B. Meijer, K. Mertens, S. Zanivan, Quantitative phosphoproteomics unveils temporal dynamics of thrombin signaling in human endothelial cells. *Blood* **123**, e22–e36 (2014).

19. M. E. Mendelsohn, Y. Zhu, S. O'Neill, The 29-kDa proteins phosphorylated in thrombin-activated human platelets are forms of the estrogen receptor-related 27-kDa heat shock protein. *Proc. Natl. Acad. Sci. U.S.A.* **88**, 11212–11216 (1991).

20. C. M. Brophy, D. Woodrum, D. Dickinson, A. Beall, Thrombin activates MAPKAP2 kinase in vascular smooth muscle. *J. Vasc. Surg.* **27**, 963–969 (1998).

21. D. Stokoe, K. Engel, D. G. Campbell, P. Cohen, M. Gaestel, Identification of MAPKAP kinase 2 as a major enzyme responsible for the phosphorylation of the small mammalian heat shock proteins. *FEBS Lett.* **313**, 307–313 (1992).

22. M. M. McLaughlin, S. Kumar, P. C. McDonnell, S. Van Horn, J. C. Lee, G. P. Livi, P. R. Young, Identification of mitogen-activated protein (MAP) kinase-activated protein kinase-3, a novel substrate of CSBP p38 MAP kinase. *J. Biol. Chem.* **271**, 8488–8492 (1996).

23. N. Ronkina, A. Kotlyarov, O. Dittrich-Breiholz, M. Kracht, E. Hitti, K. Milarski, R. Askew, S. Marusic, L. L. Lin, M. Gaestel, J. B. Telliez, The mitogen-activated protein kinase (MAPK)-activated protein kinases MK2 and MK3 cooperate in stimulation of tumor necrosis factor biosynthesis and stabilization of p38 MAPK. *Mol. Cell. Biol.* **27**, 170–181 (2007).

24. N. Ronkina, A. Kotlyarov, M. Gaestel, MK2 and MK3—A pair of isoenzymes? *Front. Biosci.* **13**, 5511–5521 (2008).

25. P. Rajagopal, Y. Liu, L. Shi, A. F. Clouser, R. E. Klevit, Structure of the α-crystallin domain from the redox-sensitive chaperone, HSPB1. *J. Biomol. NMR* **63**, 223–228 (2015).

26. L. A. Kelley, S. Mezulis, C. M. Yates, M. N. Wass, M. J. E. Sternberg, The Phyre2 web portal for protein modeling, prediction and analysis. *Nat. Protoc.* **10**, 845–858 (2015).

27. S. Y. Hwang, S. Y. Kwak, Y. Kwon, Y. S. Lee, Y. Na, Synthesis and biological effect of chrom-4-one derivatives as functional inhibitors of heat shock protein 27. *Eur. J. Med. Chem.* **139**, 892–900 (2017).

28. M. L. Kahn, M. Nakanishi-Matsui, M. J. Shapiro, H. Ishihara, S. R. Coughlin, Protease-activated receptors 1 and 4 mediate activation of human platelets by thrombin. *J. Clin. Invest.* **103**, 879–887 (1999).

29. H. Tokuda, G. Kuroyanagi, M. Tsujimoto, R. Matsushima-Nishiwaki, S. Akamatsu, Y. Enomoto, H. Iida, T. Otsuka, S. Ogura, T. Iwama, K. Kojima, O. Kozawa, Thrombin receptor-activating protein (TRAP)-activated Akt is involved in the release of phosphorylated-HSP27 (HSPB1) from platelets in DM patients. *Int. J. Mol. Sci.* **17**, 737 (2016).

30. K. Nakajima, K. Hirade, A. Ishisaki, H. Matsuno, H. Suga, Y. Kanno, E. Shu, Y. Kitajima, Y. Katagiri, O. Kozawa, Akt regulates thrombin-induced HSP27 phosphorylation in aortic smooth muscle cells: Function at a point downstream from p38 MAP kinase. *Life Sci.* **77**, 96–107 (2005).

31. B. L. van den Eshof, A. J. Hoogendijk, P. J. Simpson, F. P. J. van Alphen, S. Zanivan, K. Mertens, A. B. Meijer, M. van den Biggelaar, Paradigm of biased PAR1 (protease-activated receptor-1) activation and inhibition in endothelial cells dissected by phosphoproteomics. *Arterioscler. Thromb. Vasc. Biol.* **37**, 1891–1902 (2017).

32. L. Claesson-Welsh, Vascular permeability—The essentials. *Ups. J. Med. Sci.* **120**, 135–143 (2015).

33. A. Cuenda, S. Rousseau, p38 MAP-kinases pathway regulation, function and role in human diseases. *Biochim. Biophys. Acta* **1773**, 1358–1375 (2007).

34. P. Khanna, T. Yunkunis, H. S. Muddana, H. H. Peng, A. August, C. Dong, p38 MAP kinase is necessary for melanoma-mediated regulation of VE-cadherin disassembly. *Am. J. Physiol. Cell Physiol.* **298**, C1140–C1150 (2010).

35. T. Mirzapoiazova, I. A. Kolosova, L. Romer, J. G. Garcia, A. D. Verin, The role of caldesmon in the regulation of endothelial cytoskeleton and migration. *J. Cell. Physiol.* **203**, 520–528 (2005).

36. M. J. Rabiet, J. L. Plantier, Y. Rival, Y. Genoux, M. G. Lampugnani, E. Dejana, Thrombin-induced increase in endothelial permeability is associated with changes in cell-to-cell junction organization. *Arterioscler. Thromb. Vasc. Biol.* **16**, 488–496 (1996).

37. N. V. Bogatcheva, J. G. N. Garcia, A. D. Verin, Molecular mechanisms of thrombin-induced endothelial cell permeability. *Biochemistry (Mosc.)* **67**, 75–84 (2002).

38. V. Zakowski, G. Keramas, K. Kilian, U. R. Rapp, S. Ludwig, Mitogen-activated 3p kinase is active in the nucleus. *Exp. Cell Res.* **299**, 101–109 (2004).

39. J. Cairns, S. Qin, R. Philp, Y. H. Tan, G. R. Guy, Dephosphorylation of the small heat shock protein Hsp27 in vivo by protein phosphatase 2A. *J. Biol. Chem.* **269**, 9176–9183 (1994).

40. V. K. Pulakazhi Venu, M. Saifeddine, K. Mihara, M. El-Daly, D. Belke, J. L. E. Dean, E. R. O'Brien, S. A. Hirota, M. D. Hollenberg, Heat shock protein-27 and sex-selective regulation of muscarinic and proteinase-activated receptor 2-mediated vasodilatation: Differential sensitivity to endothelial NOS inhibition. *Br. J. Pharmacol.* **175**, 2063–2076 (2018).

41. U. J. K. Soh, J. Trejo, Activated protein C promotes protease-activated receptor-1 cytoprotective signaling through β-arrestin and dishevelled-2 scaffolds. *Proc. Natl. Acad. Sci. U.S.A.* **108**, E1372–E1380 (2011).

42. M. Renna, C. Schaffner, K. Brown, S. Shang, M. H. Tamayo, K. Hegyi, N. J. Grimsey, D. Cusens, S. Coulter, J. Cooper, A. R. Bowden, S. M. Newton, B. Kampmann, J. Helm, A. Jones, C. S. Haworth, R. J. Basaraba, M. A. DeGroote, D. J. Ordway, D. C. Rubinsztein, R. A. Floto, Azithromycin blocks autophagy and may predispose cystic fibrosis patients to mycobacterial infection. *J. Clin. Invest.* **121**, 3554–3563 (2011).

43. M. J. Ludeman, H. Kataoka, Y. Srinivasan, N. L. Esmon, C. T. Esmon, S. R. Coughlin, PAR1 cleavage and signaling in response to activated protein C and thrombin. *J. Biol. Chem.* **280**, 13122–13128 (2005).

Citation: C. C. Rada, H. Mejia-Pena, N. J. Grimsey, I. Canto Cordova, J. Olson, J. M. Wozniak, D. J. Gonzalez, V. Nizet, J. Trejo, Heat shock protein 27 activity is linked to endothelial barrier recovery after proinflammatory GPCR-induced disruption. *Sci. Signal.* **14**, eabc1044 (2021).

Heat shock protein 27 activity is linked to endothelial barrier recovery after proinflammatory GPCR-induced disruption

Cara C. RadaHilda Mejia-PenaNeil J. GrimseyIsabel Canto CordovaJoshua OlsonJacob M. WozniakDavid J. GonzalezVictor NizetJoAnn Trejo

Breaking down and building barriers

Ligand-dependent activation of proinflammatory GPCRs, such as the thrombin receptor PAR1, disrupts endothelial barriers, resulting in tissue edema. GPCR-mediated activation of the kinase p38 MAPK mediates endothelial barrier permeability. Rada *et al.* used mass spectrometry to show that the chaperone protein HSP27 was differentially phosphorylated by kinases downstream of p38 MAPK in thrombin-stimulated endothelial cells. Phosphorylation shifted HSP27 from an oligomeric to a monomeric state, resulting in enhanced endothelial barrier disruption. However, reassembly of HSP27 oligomers was required for endothelial barrier recovery. In mice, pharmacological inhibition of HSP27 function increased PAR1-induced vascular leakage. Together, these data suggest that the regulation of HSP27 phosphorylation and function affects the dynamics of endothelial barrier function.

View the article online
https://www.science.org/doi/10.1126/scisignal.abc1044
Permissions
https://www.science.org/help/reprints-and-permissions

Use of think article is subject to the Terms of service